Anodized WO_3 for Establishing Schottky based Hydrogen Gas and Ethanol Vapor Sensors

Rosmalini Ab. Kadir[a,*], *Wei Zhang*[a], *Jian Zhen Ou*[a], *Wojtek Wlodarski*[a],

Anthony P. O'Mullane[b] *and Kourosh Kalantar-zadeh*[a,*]

[a] School of Electrical and Computer Engineering, RMIT University, Melbourne, VIC 3001, Australia

[b] School of Chemistry, Physics and Mechanical Engineering, Queensland University of Technology, Brisbane, QLD 4001, Australia

* Corresponding Authors: Ms. Rosmalini Ab Kadir and Prof. Kourosh Kalantar-zadeh

Mailing Address: rosmalini@gmail.com and kourosh.kalantar@rmit.edu.au

Phone: +61-3-99253254

Fax: +61-3-99253242

ABSTRACT: This paper reports the development of nanoporous tungsten trioxide (WO_3) Schottky diode-based gas sensors. The nanoporous WO_3 films were prepared by anodic oxidation of tungsten (W) foil in ethylene glycol (98% purity) mixed with ammonium fluoride (NH_4F) and a small amount of water. Anodization resulted in highly ordered WO_3 films with a large surface to volume ratio. Utilizing these nanoporous structures, Schottky diode-based gas sensors were developed by depositing a platinum (Pt) catalytic contact and tested towards hydrogen gas and ethanol vapour. Analysis of the current–voltage (I–V) characteristics and dynamic responses of the sensors indicated that these devices exhibited a larger voltage shift in the presence of hydrogen gas compared to ethanol vapour at an optimum operating temperature of 200 °C. In addition, the gas sensing mechanism was fully discussed.

KEYWORDS: Tungsten trioxide (WO_3), anodization, nanoporous, Schottky diode, hydrogen, ethanol

1. INTRODUCTION

Tungsten trioxide (WO_3) is a *n*-type semiconductor with a band gap reported in the range of 2.6 to 3.3 eV, which has a wide range of applications due to its excellent electrical and optical properties.[1-4] Various WO_3 morphologies have been synthesized using different physical and chemical routes. Chemical routes including hydrothermal, solvothermal, anodization and thermal oxidation methods have been shown to result in various morphologies including nanowires, nanorods, nanosheets, nanoparticles, and nanoplatlets as well as nanoporous films.[5-12] The aforementioned structures have been studied for diverse applications such as electrochromic smart windows, batteries, catalysts, electronic devices and solar cells.[5-7, 11-16] WO_3 is also one of the most interesting and most researched metal oxides for sensing gases such as hydrogen (H_2), hydrogen sulfide (H_2S), hydrocarbons, ethanol (C_2H_5OH), ammonia (NH_3), nitrogen oxide (NO_2, NO and N_2O) and carbon oxide (CO).[13-14, 17-20] Many of these investigations are focused on conductometric based gas sensors, and the application of WO_3 nanostructures in contact based systems, including Schottky diode based sensors, have received rather limited attention.

The electron affinity of WO_3 is in the order of 3.2 to 4.0 eV.[21] As a result, a Schottky diode-based sensor can be developed by depositing a large work function noble metal such as Pt (work function of 5.7 eV), Au (work function of 5.4 eV) and Pd (work function of 5.6 eV) as the adjoining electrode.[22] In addition, these noble metals can act as excellent catalysts for enhancing the gas reactions and augmenting the overall performance of the sensor. The operating principles of the Schottky based sensors are primarily associated with the observation of shifts in the I–V curves caused by dissociation of the gas analyte on the catalytic metal surface which alters the Schottky barrier height at the metal-metal oxide interface.[23-25] This causes an effective change in the semiconductor work function, resulting

in a voltage change across it. This consequently changes the current through the junction as well.

The gas sensing characteristics of the Schottky contacts are greatly influenced by the morphology and porosity of the structures at the contact interface, the identity of the contact metal and the semiconducting properties of the materials.[26] The reduction of the components' morphologies to nano dimensions can also alter the behavior of the systems. Obviously, the alteration of surface energy, an increase in the surface to volume ratio, adjustments with relation to Debye length and stoichiometry of the semiconducting material are all important factors that affect the characteristics of the Schottky based sensors.[27-31] Additionally, the porosity of the semiconductor components enhances gas diffusion through the film and increases gas interaction and eventually adsorption of the gas molecules which can improve the sensor's performance.[32-33]

There are many reports regarding the development of nanoporous structures and thin films of metal oxides for improving the performance of gas sensors.[34-38] One of the most extensively investigated methods to fabricate highly porous metal oxides is anodization. Anodization generally occurs by applying a voltage across two electrodes that include one made of the base metal forming the porous metal oxide and the other a reference electrode in a suitable electrolyte. Anodization can potentially offer a simple and efficient process to obtain films with large surface area, tunable pore sizes and highly ordered morphologies.[39-42]

To the best of authors' knowledge, there is no report in the literature regarding the synthesis of WO_3 Schottky-based gas sensors via an anodization approach. Therefore, in this report, we demonstrate the performance of a WO_3 Schottky-based gas sensor prepared by anodization of W foil. The synthesis was performed in a mixed ethylene glycol-water solvent containing 0.5 g of NH_4F at room temperature. In this work, we studied and compared the performances of Schottky diode-based gas sensor towards hydrogen gas and ethanol vapour.

The sensor performances such as voltage shift, response and recovery time have been investigated and discussed in detail. The gas sensing properties of the sensors based on the synthesized nanoporous WO_3 exhibit a better response to hydrogen gas as compared to ethanol vapour.

2. EXPERIMENTAL

2.1 SYNTHESIS OF WO_3

W foil (99.9% purity) used in this work was purchased from Sigma Aldrich and cut into pieces of 1.0 cm × 1.5 cm. After the clean-up, the cut samples were anodized in an electrolyte of 50 mL ethylene glycol (98% anhydrous) mixed with 10% (wt) NH_4F (98% purity) (both from Sigma-Aldrich) and a small amount of DI water. The anodization was carried out with a conventional two electrode configuration at room temperature,[43] where the anode was the W foil piece and the cathode was a platinum foil. Anodization at a voltage of 10 V for a duration of 15 minutes resulted in WO_3 films comprising of 500 nm thick nanoporous structures. Upon the completion of the anodization experiment, samples were washed using DI water and dried in a nitrogen stream. The as-anodized samples were then annealed using a standard laboratory horizontal furnace at 500 °C for 1 h in air with a ramp-up and ramp-down rate of 2°C min^{-1} which resulted in crystalline WO_3 films.

For fabricating the gas sensors, a Pt catalytic contact with athickness of ~15 nm was deposited on top of the WO_3 nanoporous using a GATAN PECS™ (Precision Etching Coating System) thin film coater. The non-anodized side of the W substrates were used as the ohmic contact (Figure 1a).

2.2 STRUCTURAL CHARACTERIZATIONS

The films morphologies were assessed using a scanning electron microscope (SEM - FEI Nova NanoSEM), while the chemical properties of the films were investigated by X-ray photoemission spectroscopy (XPS) using a Thermo K-alpha X-ray source (1486.7 eV) with pass energy of 50 eV. The crystallinity of the WO_3 films was characterized by a D8 Advance Bruker AXS X-ray diffractor with General Area Detector Diffraction System (GADDS) attachment fitted with a 50 μm spot size collimator, incorporating a High Star 2 dimensional detector and CuKα radiation (λ = 0.1542 nm) operating at 40 kV and 40 mA. Raman spectroscopy was performed using a 532 nm laser at 0.9 mW power with a PerkinElmer Raman Station 400F.

2.3 GAS SENSING MEASUREMENTS

During the measurements, the sensors were placed in a gas testing chamber connected to the T95 controller (both from Linkam Scientific Instruments), which was capable of controlling the temperature of the device *via* an external micro heater beneath the sensors. The operating system was accessed through Linksys 32 Software Package enabling the users to quickly enter experimental parameters such as temperature and heating rate. A thermocouple is connected to the stage for measuring the sensor surface temperatures online. Detail of the measurement set-up can be seen in the schematic diagram as presented in Figure 1b. The electrical contact was formed by connecting the needle probes to the Pt electrodes of the sensors. I–V characteristics were measured using a Keithley 2600 current source meter. The gas sensor was supplied with a constant bias current (100 μA) in order to measure the dynamic response of the device when it was periodically exposed to ambient air and the analyte gas (hydrogen/ethanol) with the pulse sequence of 0.06%, 0.12%, 0.25%, 0.50% and 1%. The voltage change was recorded utilizing an Agilent 34410A digital multimeter. The concentration was accurately controlled using a computerized mass flow controller (MFC)

multi-channel gas calibration system by changing the synthetic air to analyte gas ratio while maintaining a total constant flow rate of 200 SCCM (mL/min).

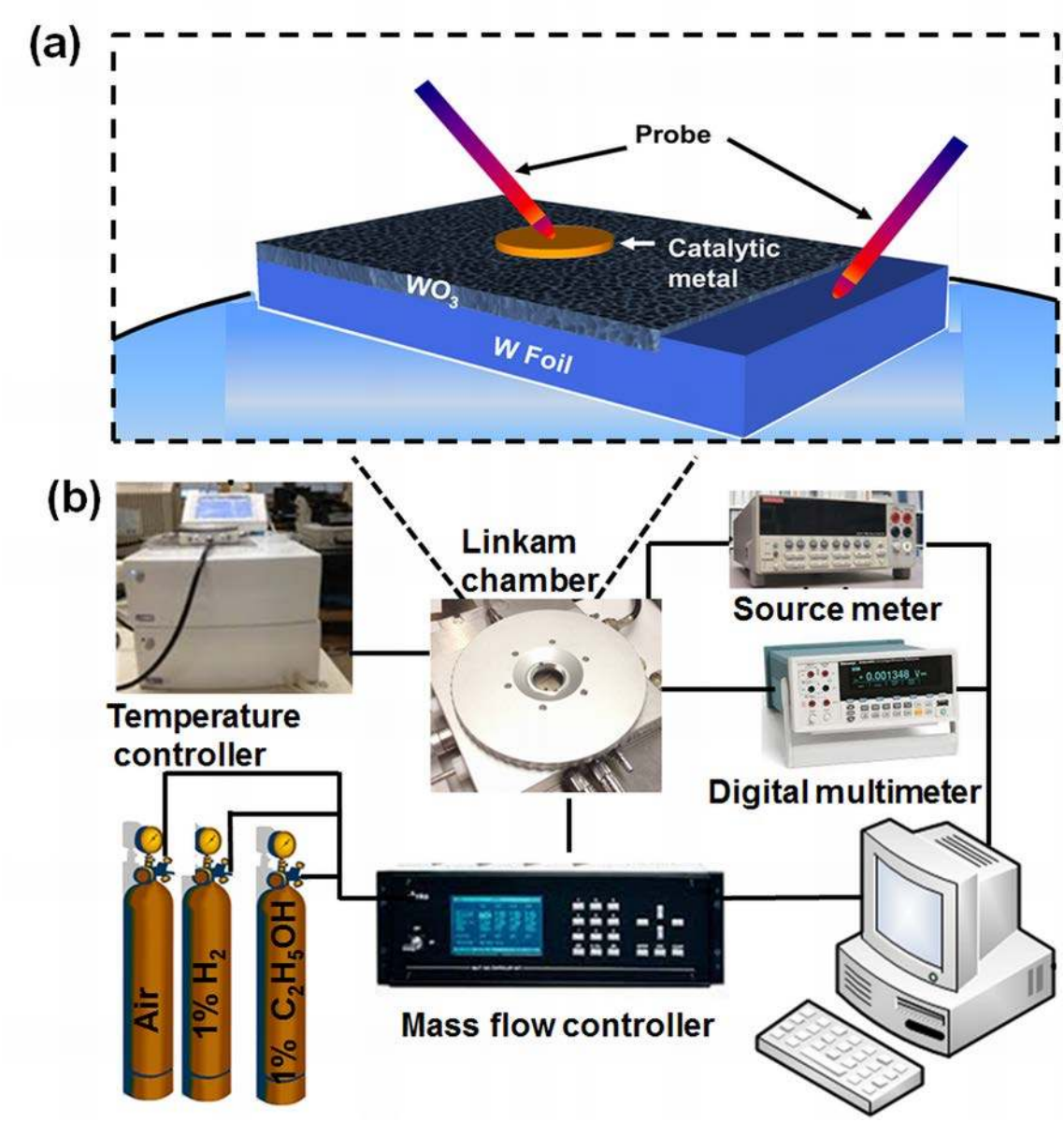

Figure 1. The schematic diagrams of (a) three-dimensional Schottky-based WO_3 sensor and (b) the gas sensing measurement set-up.

3. RESULTS AND DISCUSSION

3.1 MORPHOLOGY AND STRUCTURAL PROPERTIES

The SEM images of the as anodized and annealed WO_3 films fabricated using an anodization voltage of 10 V for 15 minutes at room temperature are presented in Figure 2. From the top-view SEM image of the WO_3 layer of Figure 2(b, c), it is evident that a highly ordered self-organized three-dimensional (3D) nanoporous layer is formed over the entire surface. This porous layer consists of a very regular structure with pores encapsulated by interconnected walls. The pores have average dimensions in the order of 10 to 30 nm and a pore wall thickness ranging from 10 to 20 nm. The magnified cross sectional image of WO_3 (Fig. 2(d)) reveals a porous film with a thickness of ~500 nm. This thickness was chosen as Rozina *et al*. have demonstrated that sensing properties can be enhanced as the thickness of anodized oxide films is decreased.[35] A thickness below 500 nm could not be implemented as a short circuit occurred while forming the Schottky contacts.

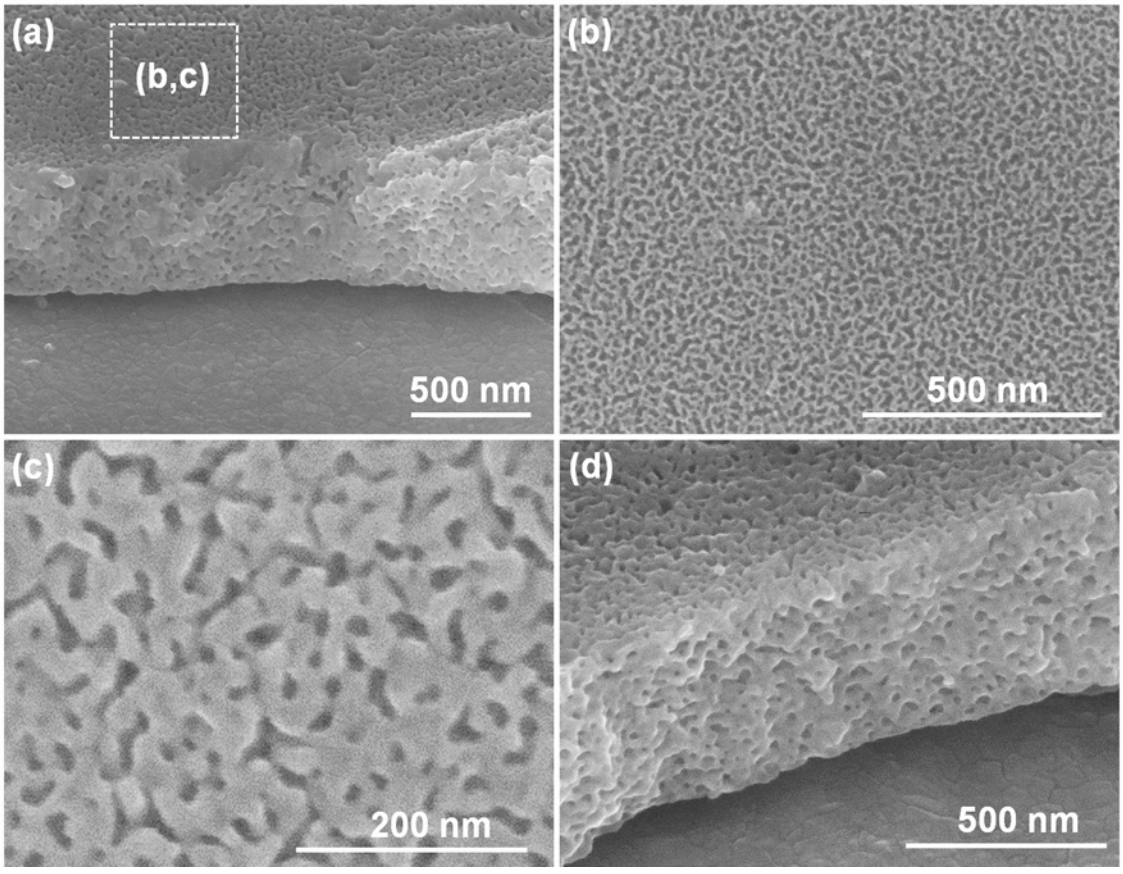

Figure 2. SEM images of anodized WO_3 (a) cross sectional view (b) top view (c) a magnified image of the interface in (b) and (d) a magnified image of cross sectional view.

In order to examine the composition of the porous WO_3 layers, XPS analysis was carried out. Figure 3a shows the XPS spectra obtained from a wide survey scan presenting peaks of W, O, N and C. The presence of carbon and nitrogen on the surface is attributed to atmospheric contamination. Figure 3b shows the high resolution core level W 4f spectra of WO_3 films. The binding energies of 35.4 and 37.9 correspond to W $4f_{7/2}$ and W $4f_{5/2}$, respectively,[44] indicating a stoichiometry WO_3 film.

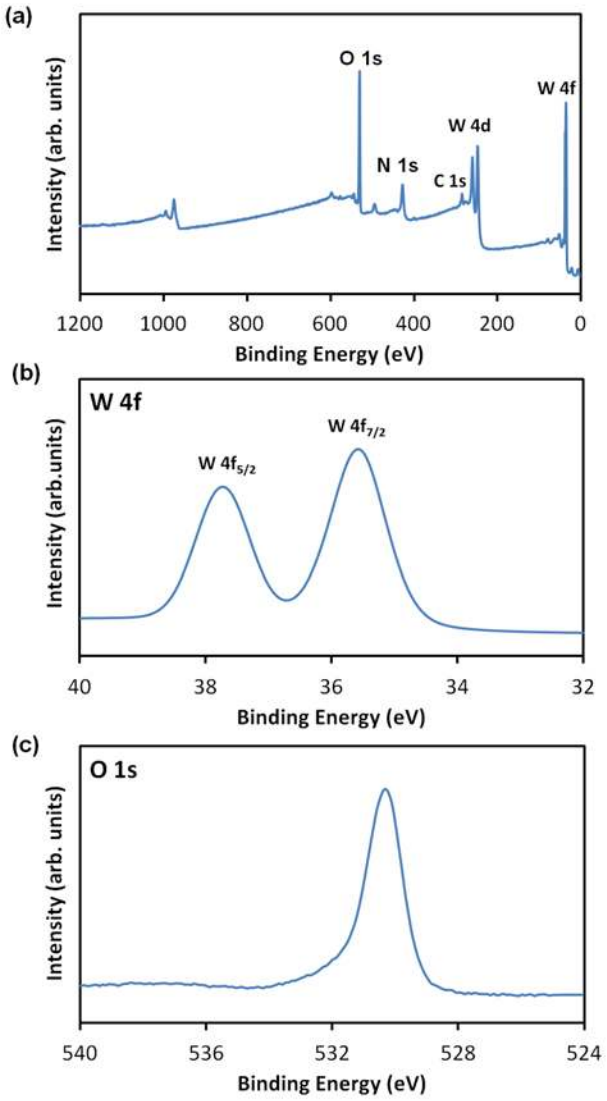

Figure 3. (a) The XPS survey scan of nanoporous WO_3 film, (b) XPS spectrum of W 4f and (c) O 1S peaks of the nanoporous WO_3 film.

Figure 4a shows the X-ray diffraction (XRD) patterns of the WO_3 films before and after annealing. The strongest diffraction peaks appear at 2θ = 23.2, 24.1, 29.5, 33.9, 42.0, 49.5 and 55.5° for the annealed sample. The peaks clearly show the crystalline signature of the orthorhombic phase (ICDD 20-1324) of WO_3, which is consistent with previous reports.[11, 45]

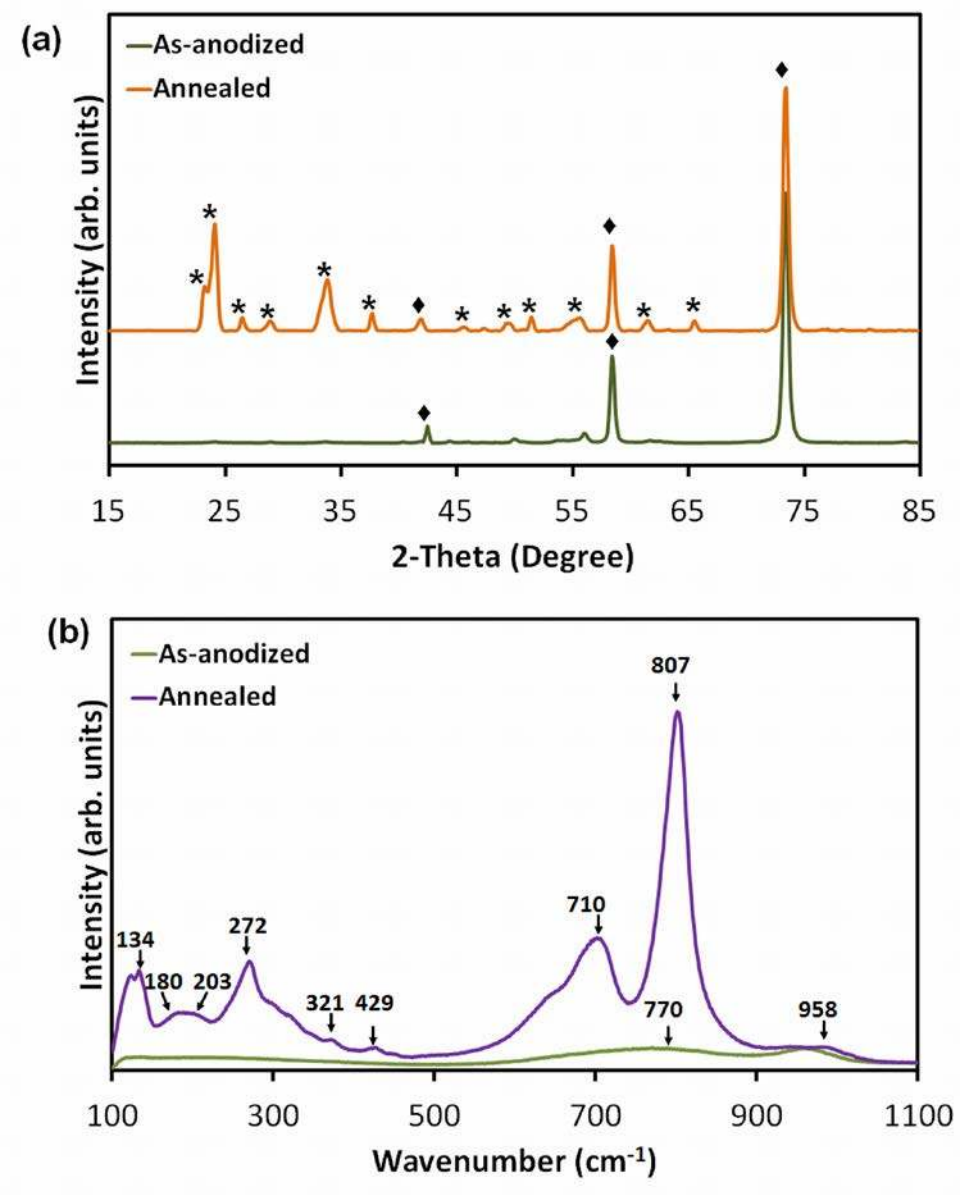

Figure 4. (a) The XRD pattern of nanoporous WO_3 film before and after annealing in air for 1 hour at 450 °C, the orthorhombic phase (ICDD 20-1324) is denoted by *, while W is denoted by ♦ and (b) the Raman spectra of the as-anodized and annealed nanoporous WO_3 films

This result was further verified by the Raman spectra presented in Figure 4b. The as-anodized WO_3 film exhibited two weak and broad Raman bands centered at 770 and 960 cm^{-1}, respectively. After annealing, new peaks appeared at 807 and 710 cm^{-1} as well as at 134 and 271 cm^{-1}, which are indicative of the O–WO_3 orthorhombic phase of the films.[11, 45] This

pattern can be assigned to either the monoclinic or orthorhombic phase, as it has been reported that the monoclinic phase of WO_3 has a very similar Raman pattern to that of the orthorhombic phase.[11] However, the orthorhombic phase is more likely as evidenced by the XRD analysis.

3.2 GAS SENSING PERFORMANCES

The current–voltage (I–V) characteristics were obtained in the presence of air and alternately with 1% hydrogen gas (Figure 5a) or ethanol vapour (Figure 5b), respectively at temperatures ranging from 50 °C to 300 °C. As the operating temperature increased, the relative change in the I-V characteristics was observed with a very good non-linear symmetrical curve which is typical of the electrical properties of these structures.[46-47] The I–V curve showed a comparatively low current at 50°C since the charge carriers have insufficient energy to overcome the barrier height energy.[48] However, as the temperature was increased, we observed a larger current flow as a result of augmentation in the carrier's energy. The increase in current can also be due to an increase in the number of electron-hole pairs as a result of higher thermal energy.[47-49] Furthermore, the changes in current were larger upon exposures to hydrogen gas compared to ethanol vapour. This is because hydrogen molecules atoms which diffuse and intercalate with WO_3 decrease the Schottky barrier height (SBH),[23] which dopes the material and results in the formation of dipoles near the junction. The joint effect can result in more carriers with sufficient energies to flow over the lowered energy barrier *via* the thermionic emission mechanism.[50-51] The mechanism of gas sensing will be discussed in detail in the following section.

As can be seen from Figure 5, the largest lateral voltage shift of the sensor towards hydrogen gas was observed at 200 °C, while for the exposure towards ethanol vapour, the largest voltage shift occurred at 300 °C. It is suggested that ethanol vapour dissociates at

catalytic metals at higher temperatures as compared to hydrogen. It has been reported that dissociation of ethanol begins at a temperature of ~55 °C and that the process is maximized at 300 °C.[52] The optimum operating temperature for the maximum voltage shift of hydrogen being lower compared to ethanol agrees well with the other previously reported Schottky-based sensors.[35-36, 53]

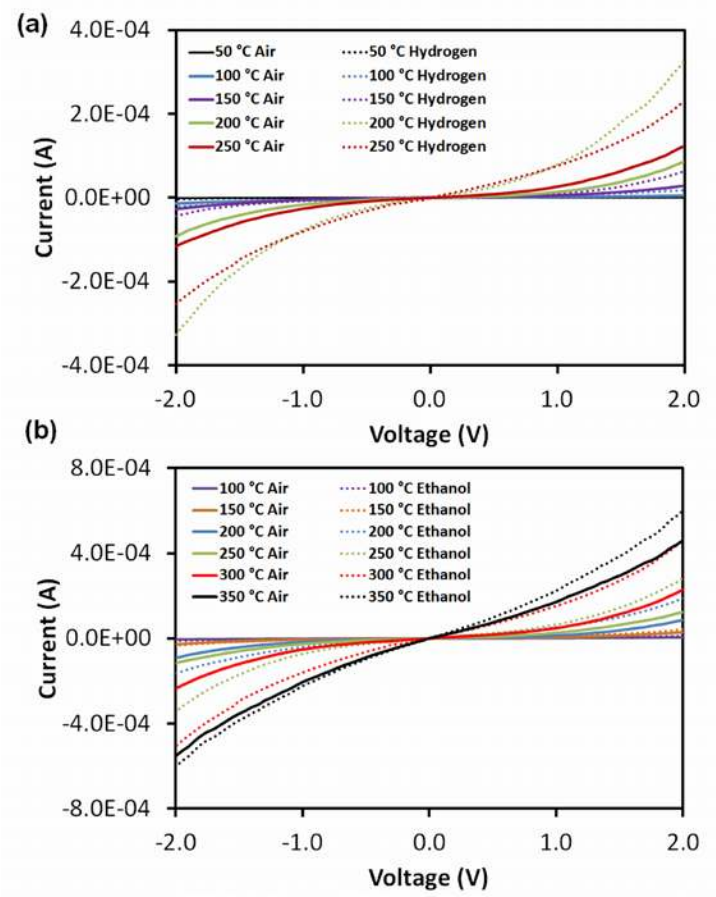

Figure 5. (a) The IV characteristics of the nanoporous WO_3 gas sensor upon exposure to (a) hydrogen gas and (b) ethanol vapour.

The different I-V response for each sensor is attributed to the reduction of the SBH, which can be calculated using the thermionic emission equation. The dependence of forward current on the applied voltage of a Schottky diode is given by the expression[47]:

$$I_F = I_s\left\{\exp\left(\frac{qV_F}{kT}\right)-1\right\} \qquad (1)$$

where I_s, q, V_F, T and k are the saturation current in ampere, the charge of one electron in Coulombs, the forward applied voltage in volts, the absolute temperature in Kelvin and the Boltzmann's constant, respectively. The I_s is defined by:

$$I_s = AA^{**}T^2 \exp\left(-\frac{q\Phi_B}{kT}\right) \quad (2)$$

in which A is the diode area in m^2, A** is the Richardson constant and Φ_B is the Schottky barrier height in eV. Using equation (2), the SBH can be determined. The SBH change in the presence of hydrogen, $\Delta\Phi_{B(H_2)} = \Phi_{B(H_2)} - \Phi_{B(Air)}$ or the SBH change in the presence of ethanol, $\Delta\Phi_{B(Eth)} = \Phi_{B(Eth)} - \Phi_{B(Air)}$ at different temperatures were calculated and shown in Table 1.

Table 1 Barrier height change at different temperatures.

Temperature (°C)	Barrier Height Change (eV)	
	Hydrogen $\Delta\Phi_{B(H_2)}$	Ethanol $\Delta\Phi_{B(Eth)}$
50	0.029	0.011
100	0.039	0.018
150	0.047	0.022
200	0.065	0.028
250	0.035	0.032
300	-	0.041
350	-	0.033

As the largest lateral voltage shifts upon exposure to hydrogen and ethanol were observed at 200 and 300 °C, respectively, the dynamic responses of the sensor were investigated at

these temperatures. The dynamic responses of the sensor with a constant bias current of 100 μA towards different concentrations of hydrogen gas and ethanol vapour, in an air background, are shown in Figure 6a and b respectively. The device demonstrated a very good response to hydrogen and ethanol at its respective optimum temperature, where the sensor's output returns to the baseline after recovery.

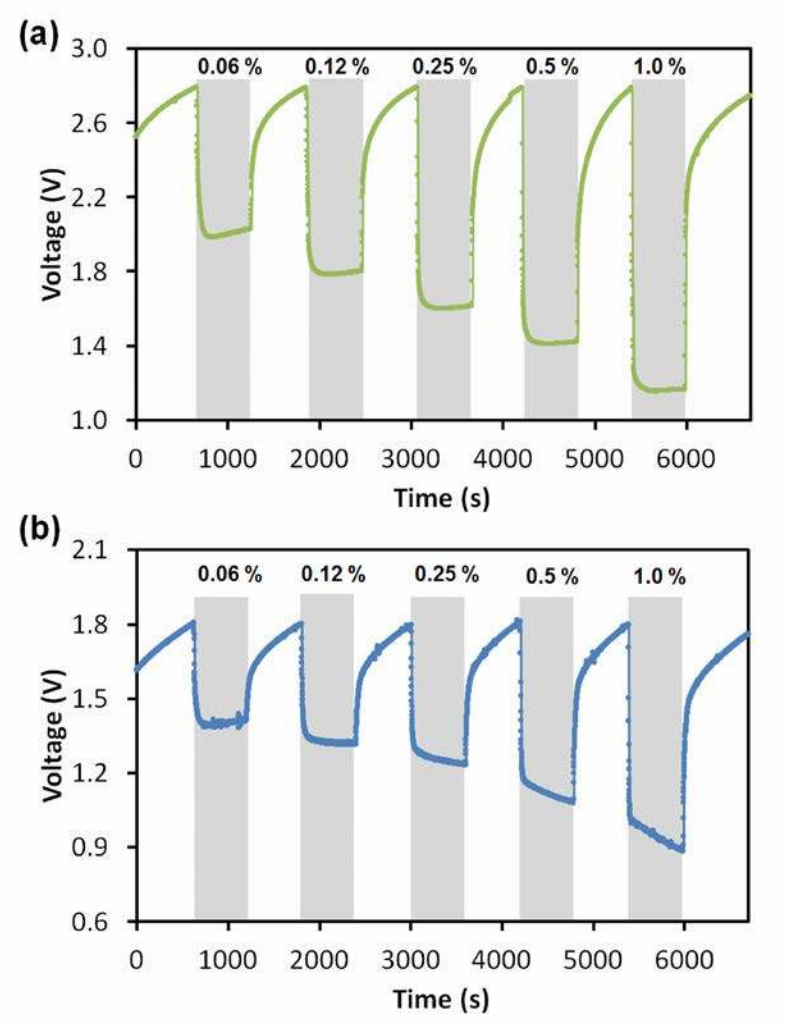

Figure 6. (a) The dynamic response of nanoporous WO_3 gas sensors measured with different concentrations of (a) H_2 gas at 200 °C and (b) ethanol vapour at 300 °C with a constant bias current of 100 μA

The stability of the sensor was investigated by repeatedly switching from air to 1 % hydrogen over a few cycles and presented in Figure 7. The sensor was found to have stable

response and recovery characteristics, indicating that high repeatability and stability were achieved. The measurements were all conducted in a non-humid environment. It is believed that humidity will certainly deteriorate the response of the device as reported previously.[36, 54]

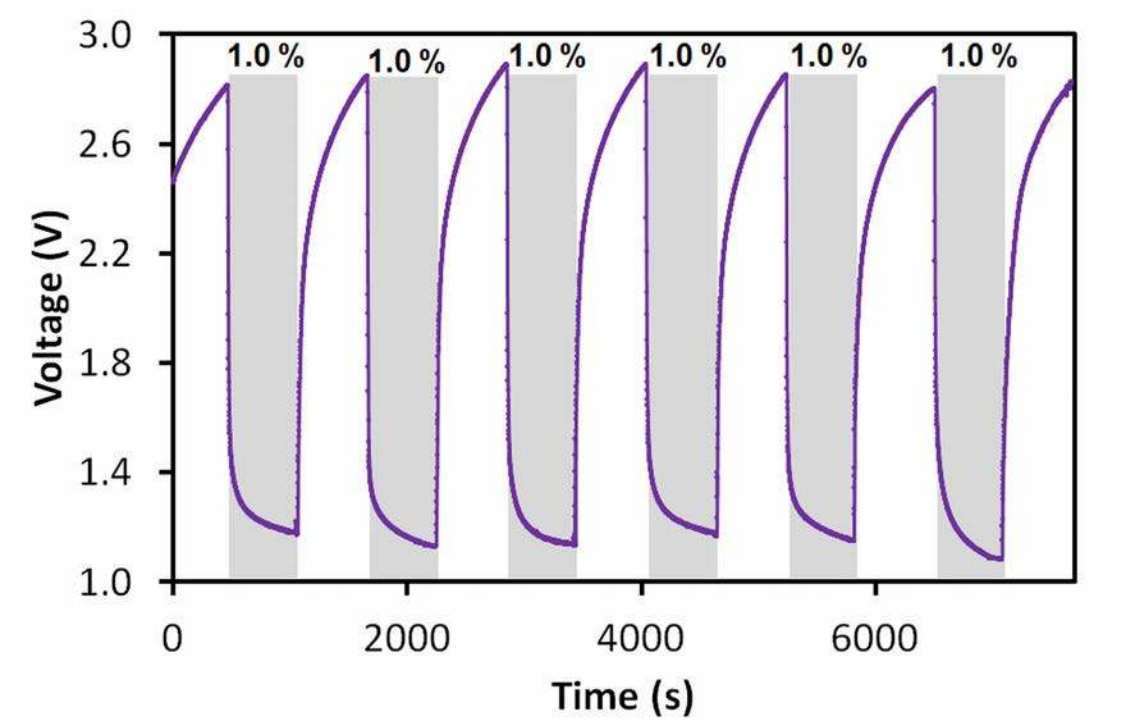

Figure 7. Reproducibility of the sensor upon exposure to hydrogen gas at 200 °C for 6 cycles.

The voltage shift in the presence of both hydrogen gas and ethanol vapour *vs* their different concentrations are presented in Figure 8. Voltage shifts of 0.77, 0.99, 1.18, 1.38 and 1.63 V were measured for 0.06, 0.125, 0.25, 0.5 and 1 % hydrogen gas, respectively. However, the same set of ethanol vapour concentration resulted in smaller voltage shifts which were 0.4, 0.46, 0.55, 0.68 and 0.79 V, respectively, as discussed previously. As the concentration of hydrogen gas increases, more hydrogen molecules will be adsorbed on the Pt catalytic surface and converted to H^+ ions. Consequently, a lower barrier height was observed resulting in a higher voltage shift. Additionally, it can be clearly seen that the sensor is more sensitive to hydrogen as compared to ethanol.

The response factor (*RF*) in percentage is defined as the ratio of the voltage shift over the base voltage in air and can be described as follows;

$$RF = \frac{V_{air} - V_{gas}}{V_{air}} \text{x} 100\% \quad (3)$$

The gas sensor response factors were calculated as 27.5, 35.35, 42.14, 49.28 and 58.21% for the aforementioned hydrogen gas concentration while for ethanol vapour with the same set of concentration the response factors were 22.22, 25.56, 30.56, 37.78 and 43.89 %.

.

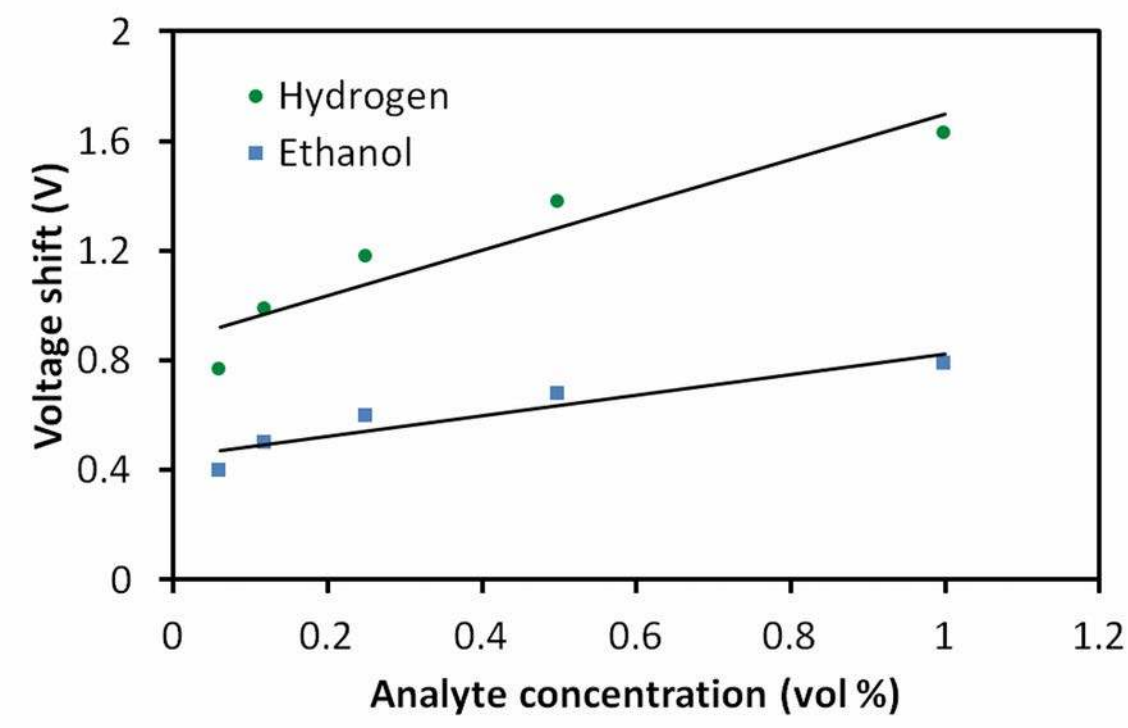

Figure 8. Voltage shifts recorded with nanoporous WO_3 gas sensors at different concentrations of target gas.

We further evaluated the performance of the WO_3 gas sensor in terms of the response and recovery time. The response time is defined as the time required for 90% of the total voltage change and the recovery time is the time taken for 90% recovery of the total voltage change. Response and recovery times were obtained for the nanoporous WO_3 Schottky diode sensor

when exposed alternately to synthetic air with a hydrogen or ethanol balance concentration in the order of 0.06 - 1% and the data is shown in Table 2. The sensor's recovery time is about 4 times longer than the response time. The same trend of response and recovery time for other nanoporous metal oxide gas sensors have been reported where the recovery time is generally longer than the response time upon exposure to a variety of analytes.[35, 55] As the concentration of gas analyte increases, a faster response is demonstrated. Conversely, the recovery time increases as the gas analyte concentration increases. It is suggested that, at higher concentrations of the target gas, a larger number of target gas molecules dissociate on the catalytic metal and adsorb inside the porous film.[56] As a result, a faster response is observed compared to the response of the target gas at lower concentration. However, purging the target gas out from the nanoporous films takes a longer time as the concentration of the target gas in the films results in larger stoichiometry changes within the films, which require longer recovery times to return to its initial condition.

Table 2 Response and recovery time of the sensor at different analyte concentrations.

Analyte concentration (vol %)	Hydrogen		Ethanol	
	Response time (s)	Recovery time (s)	Response time (s)	Recovery time (s)
0.06	43	108	55	128
0.12	38	111	42	139
0.25	29	124	32	153
0.5	23	151	27	172
1.0	20	180	25	185

A shorter response time is observed upon hydrogen exposure in comparison with the response to ethanol. Hydrogen gas dissociates directly to produce hydrogen ions, while ethanol vapour needs an additional dehydrogenation step where ethanol dissociates into

ethoxides and acetaldehyde before generating hydrogen ions.[57-58] Thus, the device demonstrated a longer response time upon exposure to ethanol vapour.

The sensing mechanism of the nanoporous WO_3 gas sensor is explained as follows. Dissociative chemisorption of molecular hydrogen onto Pt, forming hydrogen ions (H^+) and electrons (e^-) is described by [59]:

$$H_2(g) \rightarrow 2H^+ + 2e^- \quad (4)$$

Similarly, on the catalyst surface, ethanol molecules start to dissociate into ethoxides and further oxidize into acetaldehyde as in equation (4) and (5) when the temperature increases.[60]:

$$C_2H_5OH(g) \rightarrow CH_3CH_2O + H(a) \quad (5)$$

$$C_2H_5O(a) \rightarrow CH_3CHO(g) + H(a) \quad (6)$$

in which (g) and (a) stand for the gaseous and adsorbed species, respectively. The H atoms produced from equation (5) and (6) are oxidized to H^+ with the liberation of an electron e^-, resulting in adsorbed H^+.

The accumulated $H^+_{(ads)}$ ions from equation (3) to (5) diffuse over the catalytic metal and intercalate with the WO_3 pore wall that can be described according to the following formula[5]:

$$WO_3 + xH^+ + xe^- \leftrightharpoons H_xWO_3 \quad (7)$$

The released electrons in equation (7) reduce the width of the depletion region in the oxide film, which decreases the resistance of the film and also the barrier height that corresponds to the voltage shift for the gas sensor.[59]

As the system is maintained at an elevated temperature, it is also possible that H_xWO_3 breaks down into reduced WO_3 producing H_2O vapour.[61]

$$2H_xWO_3 \leftrightharpoons xH_2O + 2WO_{3-x/2} \quad (8)$$

Upon exposing the sensors back to air (oxygen rich environment) the reduced oxide is restored to WO_3 via:

$$WO_{3-x/2} + (x/4)O_2 \leftrightharpoons WO_3 \quad (9)$$

which allows the gas sensor to be used repeatedly.

4. CONCLUSIONS

In this work, we successfully synthesized highly ordered nanoporous WO_3 films *via* the electrochemical anodization of W. Pt was deposited as a Schottky forming contact, which also provided catalytic properties for sensing hydrogen gas and ethanol vapor. The structural properties of WO_3 films were investigated using SEM, XRD, XPS and Raman spectroscopy demonstrating the existence of an orthorhombic crystal phase made of pores in the order of 10 to 30 nm in dimensions. The Pt/WO_3 Schottky-based gas sensor was tested towards hydrogen and ethanol molecules in gaseous environments. The porosity of the WO_3 structure resulted in a high surface to volume ratio film that facilitated the adsorption/desorption of gas molecules. Gas sensing measurements for the device exhibited the best performance towards hydrogen providing a voltage shift of 1.67 V for 1% hydrogen, when the device was biased at a current of 100 μA and was operated at 200 °C. The WO_3 nanoporous Schottky gas sensor also exhibitedgood reproducibility and repeatable responses with a stable baseline.

AUTHOR INFORMATION

Corresponding Author

*Email: rosmalini@gmail.com and kourosh.kalantar@rmit.edu.au

Notes

The authors declare no competing financial interest.

ACKNOWLEDGEMENTS

The authors acknowledge the facilities, and the scientific and technical assistance, of the Australian Microscopy & Microanalysis Research Facility at the RMIT Microscopy & Microanalysis Facility (RMMF), at RMIT University

REFERENCES

1. Zheng, H.; Ou, J. Z.; Strano, M. S.; Kaner, R. B.; Mitchell, A.; Kalantar-zadeh, K., Nanostructured Tungsten Oxide - Properties, Synthesis and Applications. *Adv. Funct. Mater.* **2011**, *21*, 2175-2196.

2. Deb, S. K., Opportunities and Challenges in Science and Technology of WO_3 for Electrochromic and Related Applications. *Sol. Energ. Mat. Sol. C* **2008**, *92*, 245-258.

3. Gillet, M.; Aguir, K.; Lemire, C.; Gillet, E.; Schierbaum, K., The Structure and Electrical Conductivity of Vacuum-Annealed WO_3 Thin Films. *Thin Solid Films* **2004**, *467*, 239-246.

4. Watanabe, H.; Fujikata, K.; Oaki, Y.; Imai, H., Band-Gap Expansion of Tungsten Oxide Quantum Dots Synthesized in Sub-Nano Porous Silica. *Chem. Commun.* **2013**, *49*, 8477-8479.

5. Ou, J. Z.; Balendhran, S.; Field, M. R.; McCulloch, D. G.; Zoolfakar, A. S.; Rani, R. A.; Zhuiykov, S.; O'Mullane, A. P.; Kalantar-zadeh, K., The Anodized Crystalline WO_3 Nanoporous Network with Enhanced Electrochromic Properties. *Nanoscale* **2012**, *4*, 5980-5988.

6. Sadek, A. Z., et al., High-Temperature Anodized WO_3 Nanoplatelet Films for Photosensitive Devices. *Langmuir* **2009**, *25*, 9545-9551.

7. Cao, B.; Chen, J.; Tang, X.; Zhou, W., Growth of Monoclinic WO_3 Nanowire Array for Highly Sensitive NO_2 Detection. *J. Mater. Chem.* **2009**, *19*, 2323-2327.

8. Gu, Z.; Zhai, T.; Gao, B.; Sheng, X.; Wang, Y.; Fu, H.; Ma, Y.; Yao, J., Controllable Assembly of WO_3 Nanorods/Nanowires into Hierarchical Nanostructures. *J. Phys. Chem. B* **2006**, *110*, 23829-23836.

9. Choi, H. G.; Jung, Y. H.; Kim, D. K., Solvothermal Synthesis of Tungsten Oxide Nanorod/Nanowire/Nanosheet. *J. Am. Ceram. Soc.* **2005**, *88*, 1684-1686.

10. Zhang, J.; Tu, J.-p.; Xia, X.-h.; Wang, X.-l.; Gu, C.-d., Hydrothermally Synthesized WO_3 Nanowire Arrays with Highly Improved Electrochromic Performance. *J. Mater. Chem.* **2011**, *21*, 5492-5498.

11. Ou, J. Z.; Rani, R. A.; Balendhran, S.; Zoolfakar, A. S.; Field, M. R.; Zhuiykov, S.; O'Mullane, A. P.; Kalantar-zadeh, K., Anodic Formation of a Thick Three-Dimensional Nanoporous WO_3 Film and Its Photocatalytic Property. *Electrochem. Commun.* **2013**, *27*, 128-132.

12. Zeng, J.; Hu, M.; Wang, W.; Chen, H.; Qin, Y., NO_2 Sensing Properties of Porous WO_3 Gas Sensor Based on Anodized Sputtered Tungsten Thin Film. *Sens. Actuators B* **2012**, *161*, 447-452.

13. Ou, J. Z.; Ahmad, M. Z.; Latham, K.; Kalantar-zadeh, K.; Sberveglieri, G.; Wlodarski, W., Synthesis of the Nanostructured WO_3 Via Anodization at Elevated Temperature for H_2 Sensing Applications. *Procedia Engineering* **2011**, *25*.

14. Rout, C. S.; Ganesh, K.; Govindaraj, A.; Rao, C. N. R., Sensors for the Nitrogen Oxides, NO_2, NO and N_2O, Based on In_2O_3 and WO_3 Nanowires. *Appl. Phys. A-Mater.* **2006**, *85*, 241-246.

15. Xue, X.-Y.; He, B.; Yuan, S.; Xing, L.-L.; Chen, Z.-H.; Ma, C.-H., SnO_2/WO_3 Core-Shell Nanorods and Their High Reversible Capacity as Lithium-Ion Battery Anodes. *Nanotechnology* **2011**, *22*.

16. Zheng, H.; Tachibana, Y.; Kalantar-zadeh, K., Dye-Sensitized Solar Cells Based on WO_3. *Langmuir* **2010**, *26*, 19148-19152.

17. Ippolito, S. J.; Kandasamy, S.; Kalantar-zadeh, K.; Wlodarski, W., Hydrogen Sensing Characteristics of WO_3 Thin Film Conductometric Sensors Activated by Pt and Au Catalysts. *Sens. Actuators B* **2005**, *108*, 154-158.

18. Ahsan, M.; Ahmad, M. Z.; Tesfamichael, T.; Bell, J.; Wlodarski, W.; Motta, N., Low Temperature Response of Nanostructured Tungsten Oxide Thin Films toward Hydrogen and Ethanol. *Sens. Actuators B* **2012**, *173*, 789-796.

19. Ahmad, M. Z.; Sadek, A. Z.; Ou, J. Z.; Yaacob, M. H.; Latham, K.; Wlodarski, W., Facile Synthesis of Nanostructured WO_3 Thin Films and Their Characterization for Ethanol Sensing. *Mater. Chem. Phys.* **2013**, *141*, 912-919.

20. Siciliano, T.; Tepore, A.; Micocci, G.; Serra, A.; Manno, D.; Filippo, E., WO_3 Gas Sensors Prepared by Thermal Oxidization of Tungsten. *Sens. Actuators B* **2008**, *133*, 321-326.

21. Walter, C. W.; Hertzler, C. F.; Devynck, P.; Smith, G. P.; Peterson, J. R., Photodetachment of Wo_3 : The Electron Affinity of WO_3. *J. Chem. Phys.* **1991**, *95*, 824-827.

22. Skriver, H. L.; Rosengaard, N. M., Surface Energy and Work Function of Elemental Metals. *Phys. Rev. B* **1992**, *46*, 7157-7168.

23. Lundström, I.; Shivaraman, S.; Svensson, C.; Lundkvist, L., A Hydrogen−Sensitive Mos Field−Effect Transistor. *Appl. Phys. Lett.* **1975**, *26*, 55-57.

24. Yamamoto, N.; Tonomura, S.; Matsuoka, T.; Tsubomura, H., A Study on a Palladium-Titanium Oxide Schottky Diode as a Detector for Gaseous Components. *Surf. Sci.* **1980**, *92*, 400-406.

25. Lundstrom, K. I.; Shivaraman, M. S.; Svensson, C. M., A Hydrogen Sensitive Pd-Gate MOS Transistor. *J. Appl. Phys.* **1975**, *46*, 3876-3881.

26. Bourenane, K.; Keffous, A.; Nezzal, G.; Bourenane, A.; Boukennous, Y.; Boukezzata, A., Influence of Thickness and Porous Structure of SiC Layers on the Electrical Properties of Pt/SiC-pSi and Pd/SiC-pSi Schottky Diodes for Gas Sensing Purposes. *Sens. Actuators B* **2008**, *129*, 612-620.

27. Yu, J.; Ippolito, S. J.; Wlodarski, W.; Strano, M.; Kalantar-zadeh, K., Nanorod Based Schottky Contact Gas Sensors in Reversed Bias Condition. *Nanotechnology* **2010**, *21*.

28. Sun, Y.-F.; Liu, S.-B.; Meng, F.-L.; Liu, J.-Y.; Jin, Z.; Kong, L.-T.; Liu, J.-H., Metal Oxide Nanostructures and Their Gas Sensing Properties: A Review. *Sensors* **2012**, *12*, 2610-2631.

29. Wei, T.-Y.; Yeh, P.-H.; Lu, S.-Y.; Lin-Wang, Z., Gigantic Enhancement in Sensitivity Using Schottky Contacted Nanowire Nanosensor. *J. Am. Chem. Soc.* **2009**, *131*, 17690-17695.

30. Schierbaum, K. D.; Kirner, U. K.; Geiger, J. F.; Göpel, W., Schottky-Barrier and Conductivity Gas Sensors Based Upon Pd/SnO_2 and Pt/TiO_2. *Sens. Actuators B* **1991**, *4*, 87-94.

31. Shimizu, Y.; Egashira, M., Basic Aspects and Challenges of Semiconductor Gas Sensors. *MRS Bulletin* **1999**, *24*, 18-24.

32. Wagner, T.; Haffer, S.; Weinberger, C.; Klaus, D.; Tiemann, M., Mesoporous Materials as Gas Sensors. *Chem. Soc. Rev.* **2013**, *42*, 4036-4053.

33. Hyodo, T.; Shimizu, Y.; Egashira, M., Design of Mesoporous Oxides as Semiconductor Gas Sensor Materials. *Electrochemistry* **2003**, *71*, 387-393.

34. Hossein-Babaei, F.; Abbaszadeh, S.; Esfahani, M. S., Gas Sensitive Porous Silver-Rutile High-Temperature Schottky Diode on Thermally Oxidized Titanium. *IEEE Sens. J.* **2009**, *9*, 237-243.

35. Rani, R. A.; Zoolfakar, A. S.; Ou, J. Z.; Field, M. R.; Austin, M.; Kalantar-zadeh, K., Nanoporous Nb_2O_5 Hydrogen Gas Sensor. *Sens. Actuators B* **2013**, *176*, 149-156.

36. Kadir, R. A.; Rani, R. A.; Zoolfakar, A. S.; Ou, J. Z.; Shafiei, M.; Wlodarski, W.; Kalantar-zadeh, K., Nb_2O_5 Schottky Based Ethanol Vapour Sensors: Effect of Metallic Catalysts. *Sens. Actuators B* **2014**, *202*, 74-82.

37. Salehi, A.; Nikfarjam, A.; Kalantari, D. J., Pd/Porous-GaAs Schottky Contact for Hydrogen Sensing Application. *Sens. Actuators B* **2006**, *113*, 419-427.

38. Salehi, A.; Kalantari, D. J., Characteristics of Highly Sensitive Au/Porous-GaAs Schottky Junctions as Selective CO and NO Gas Sensors. *Sens. Actuators B* **2007**, *122*, 69-74.

39. Macak, J. M.; Tsuchiya, H.; Ghicov, A.; Yasuda, K.; Hahn, R.; Bauer, S.; Schmuki, P., TiO_2 Nanotubes: Self-Organized Electrochemical Formation, Properties and Applications. *Curr. Opin. Solid St. M.* **2007**, *11*, 3-18.

40. Masuda, H.; Hasegwa, F.; Ono, S., Self-Ordering of Cell Arrangement of Anodic Porous Alumina Formed in Sulfuric Acid Solution. *J. Electrochem. Soc.* **1997**, *144*, L127-L130.

41. Prakasam, H. E.; Shankar, K.; Paulose, M.; Varghese, O. K.; Grimes, C. A., A New Benchmark for TiO_2 Nanotube Array Growth by Anodization. *J. Phys. Chem. C* **2007**, *111*, 7235-7241.

42. Pandey, B.; Thapa, P. S.; Higgins, D. A.; Ito, T., Formation of Self-Organized Nanoporous Anodic Oxide from Metallic Gallium. *Langmuir* **2012**, *28*, 13705-13711.

43. Zheng, H.; Sadek, A. Z.; Latham, K.; Kalantar-Zadeh, K., Nanoporous WO_3 from Anodized Rf Sputtered Tungsten Thin Films. *Electrochem. Commun.* **2009**, *11*, 768-771.

44. Ou, J. Z.; Yaacob, M. H.; Breedon, M.; Zheng, H. D.; Campbell, J. L.; Latham, K.; Plessis, J. d.; Wlodarski, W.; Kalantar-zadeh, K., In Situ Raman Spectroscopy of H_2 Interaction with WO_3 Films. *Phys. Chem. Chem. Phys.* **2011**, *13*, 7330-7339.

45. Kalantar-zadeh, K.; Vijayaraghavan, A.; Ham, M.-H.; Zheng, H.; Breedon, M.; Strano, M. S., Synthesis of Atomically Thin WO_3 Sheets from Hydrated Tungsten Trioxide. *Chem. Mater.* **2010**, *22*, 5660-5666.

46. Chiu, S.-Y.; Huang, H.-W.; Huang, T.-H.; Liang, K.-C.; Liu, K.-P.; Tsai, J.-H.; Lour, W.-S., Comprehensive Study of Pd/Gan Metal-Semiconductor-Metal Hydrogen Sensors with Symmetrically Bi-Directional Sensing Performance. *Sens. Actuators B* **2009**, *138*, 422-427.

47. Sze, S. M.; Ng, K. K., *Physics of Semiconductor Devices*, 3rd ed.; Hoboken, NJ, USA: John Wiley & Sons, Inc, 2007.

48. Xu, J. P.; Lai, P. T.; Zhong, D. G.; Chan, C. L., Improved Hydrogen-Sensitive Properties of MISiC Schottky Sensor with Thin NO-Grown Oxynitride as Gate Insulator. *IEEE Electron Device L.* **2003**, *24*, 13-15.

49. Shafiei, M.; Yu, J.; Arsat, R.; Kalantar-zadeh, K.; Comini, E.; Ferroni, M.; Sberveglieri, G.; Wlodarski, W., Reversed Bias Pt/Nanostructured ZnO Schottky Diode with Enhanced Electric Field for Hydrogen Sensing. *Sens. Actuators B* **2010**, *146*, 507-512.

50. Pitcher, S.; Thiele, J. A.; Ren, H.; Vetelino, J. F., Current/Voltage Characteristics of a Semiconductor Metal Oxide Gas Sensor. *Sens. Actuators B* **2003**, *93*, 454-462.

51. Tsai, T.-H.; Huang, J.-R.; Lin, K.-W.; Hsu, W.-C.; Chen, H.-I.; Liu, W.-C., Improved Hydrogen Sensing Characteristics of a Pt/SiO_2/GaN Schottky Diode. *Sens. Actuators B* **2008**, *129*, 292-302.

52. Alonso, C. G.; Furtado, A. C.; Cantao, M. P.; dos Santos, O. A. A.; Fernandes-Machado, N. R. C., Temperature Effect on Hydrogen Production from Reactions between Ethanol and Steam in the Presence of Pd-Ru/Nb_2O_5-TiO_2 Catalyst. *Int. J. Chem. React. Eng.* **2009**, *7*.

53. Xing, L.-L.; He, B.; Chen, Z.-H.; Xue, X.-Y., Schottky Barrier and Catalytic Effect Induced High Gas Sensing of One-Step Synthesized Pd-SnO_2 Nanorods. *Solid State Sci.* **2013**, *15*, 42-46.

54. Talazac, L.; Barbarin, F.; Varenne, C.; Mazet, L.; Pellier, S.; Soulier, C., Gas Sensing Properties of Pseudo-Schottky Diodes on P-type Indium Phosphide Substrates - Application to O_3 and NO_2 Monitoring in Urban Ambient Air. *Sens. Actuators B* **2002**, *83*, 149-159.

55. Yamamoto, G.; Yamashita, T.; Matsuo, K.; Hyodo, T.; Shimizu, Y., Effects of Polytetrafluoroethylene or Polyimide Coating on H_2 Sensing Properties of Anodized TiO_2 Films Equipped with Pd–Pt Electrodes. *Sens. Actuators B* **2013**, *183*, 253-264.

56. Liu, Y.; Yu, J.; Lai, P. T., Investigation of WO_3/ZnO Thin-Film Heterojunction-Based Schottky Diodes for H_2 Gas Sensing. *Int. J. Hydrogen Energ.* **2014**, *39*, 10313-10319.

57. Ivanovskaya, M.; Kotsikau, D.; Faglia, G.; Nelli, P.; Irkaev, S., Gas-Sensitive Properties of Thin Film Heterojunction Structures Based on Fe_2O_3-In_2O_3 Nanocomposites. *Sens. Actuators B* **2003**, *93*, 422-430.

58. Han, G.; Lu, Q.; Liu, G.; Ye, X.; Lin, S.; Song, Y.; Liu, B.; Yang, X.; Li, G., Enhanced Ethanol Sensing Properties Based on A-Fe_2O_3/In_2O_3 Hollow Microspheres. *J. Mater. Sci-Mater. El* **2012**, *23*, 1616-1620.

59. Hübert, T.; Boon-Brett, L.; Black, G.; Banach, U., Hydrogen Sensors – a Review. *Sens. Actuators B* **2011**, *157*, 329-352.

60. Sexton, B. A.; Rendulic, K. D.; Huges, A. E., Decomposition Pathways of C_1-C_4 Alcohols Adsorbed on Platinum (111). *Surf. Sci.* **1982**, *121*, 181-198.

61. Yaacob, M. H.; Breedon, M.; Kalantar-zadeh, K.; Wlodarski, W., Absorption Spectral Response of Nanotextured WO_3 Thin Films with Pt Catalyst Towards H_2. *Sens. Actuators B* **2009**, *137*, 115-120.